frontiers | Frontiers in Nanotechnology

TYPE Original Research
PUBLISHED 02 May 2025
DOI 10.3389/fnano.2025.1553976

OPEN ACCESS

EDITED BY
Satyabrata Mohapatra,
Guru Gobind Singh Indraprastha University, India

REVIEWED BY
Mohan Varkolu,
Koneru Lakshmaiah Education Foundation, India
Praveen Kumar,
Indian Association for the Cultivation of Science (IACS), India

*CORRESPONDENCE
Antonija Grubišić-Čabo,
a.grubisic-cabo@rug.nl

RECEIVED 31 December 2024
ACCEPTED 24 March 2025
PUBLISHED 02 May 2025

CITATION
Dan Z, Sarmasti Emami R, Feraco G, Vavali M, Gerlach D, Sarott MF, Zhu Y, Rudolf P and Grubišić-Čabo A (2025) Role of chalcogen atoms in in situ exfoliation of large-area 2D semiconducting transition metal dichalcogenides.
Front. Nanotechnol. 7:1553976.
doi: 10.3389/fnano.2025.1553976

Role of chalcogen atoms in in situ exfoliation of large-area 2D semiconducting transition metal dichalcogenides

Zhiying Dan[1], Ronak Sarmasti Emami[1], Giovanna Feraco[1], Melina Vavali[1,2], Dominic Gerlach[1], Martin F Sarott[1,3], Yindi Zhu[1], Petra Rudolf[1] and Antonija Grubišić-Čabo[1]*

[1]Zernike Institute for Advanced Materials, University of Groningen, Groningen, Netherlands, [2]Sorbonne Université, CNRS, MONARIS, UMR 8233, Paris, France, [3]Groningen Cognitive Systems and Materials Center (CogniGron), University of Groningen, Groningen, Netherlands

Two-dimensional (2D) transition metal dichalcogenides have emerged as a promising platform for next-generation optoelectronic and spintronic devices. Mechanical exfoliation using adhesive tape remains the dominant method for preparing 2D materials of highest quality, including transition metal dichalcogenides, but always results in small-sized flakes. This limitation poses a significant challenge for investigations and applications where large scale flakes are needed. To overcome these constraints, we explored the preparation of 2D WS_2 and WSe_2 using a recently developed kinetic *in situ* single-layer synthesis method (KISS). In particular, we focused on the influence of different substrates, Au and Ag, and chalcogen atoms, S and Se, on the yield and quality of the 2D films. The crystallinity and spatial morphology of the 2D films were characterized using optical microscopy and atomic force microscopy, providing a comprehensive assessment of exfoliation quality. Low-energy electron diffraction verified that there is no preferential orientation between the 2D film and the substrate, while optical microscopy revealed that WSe_2 consistently outperformed WS_2 in producing large monolayers, regardless of the substrate used. Finally, X-ray diffraction and X-ray photoelectron spectroscopy demonstrate that no covalent bonds are formed between the 2D material and the underlying substrate. These results identify KISS method as a non-destructive method for a more scalable approach of high-quality 2D transition metal dichalcogenides.

KEYWORDS

2D materials, exfoliation, KISS, XPS, LEED, transition metal dichalcogenides

1 Introduction

In recent years two-dimensional (2D) materials have gained significant attention due to their unique electronic and optical properties, such as the transition from an indirect to a direct band gap when going from bulk to a single layer of MoS_2, which makes them highly promising for electronic, optoelectronic and spintronic devices (Pirker et al., 2024; Georgiou et al., 2013; Li et al., 2024; Zatko et al., 2019; Ellis et al., 2011). Despite their potential, the efficient and scalable production of high-quality monolayers remains a significant challenge. Mechanical exfoliation (ME), which uses adhesive tape, is widely recognized for producing high-quality flakes; however, the size of these flakes is usually on the order of

tens of micrometers, making them inadequate for many surface science studies and practical applications. Chemical vapor deposition (CVD), on the other hand, can be used to synthesize wafer-sized monolayers (Kim et al., 2020), but it involves complex optimization processes, requires high temperature conditions, and often results in monolayers with high defect density and lower quality compared to ME. Additionally, CVD lacks the universality of ME in its applicability to various 2D materials. Molecular beam epitaxy (MBE) also suffers from similar drawbacks (Schütze et al., 2024), including the need for stringent optimization of growth parameters and challenges in achieving defect-free monolayers. As a result, ME, which enables the easy separation of monolayers with distinct optical and electronic properties from the bulk transition metal dichalcogenides (TMDCs), remains a fundamental technique in both research and development of next-generation nanodevices. Furthermore, due to its simplicity, efficiency, low cost, and ability to produce high-quality monolayers, it is likely to remain one of the most widely used methods (Huang et al., 2020). However, in addition to the heterogeneous interlayer forces and surface interactions that often restrict flake sizes to tens of micrometers, ME also suffers from poor yield (Islam et al., 2022), resulting in a dramatic variations in the thickness and quality of exfoliated layers over the whole substrate touched by the adhesive tape.

The challenges are further exacerbated when handling air- or moisture-sensitive 2D materials, such as black phosphorus and VSe_2, which degrade rapidly when exposed to ambient conditions (Carré et al., 2024; Kezilebieke et al., 2020). To address these issues, ambient-sensitive materials must be handled in controlled environments, such as glove boxes, further complicating the exfoliation process (Buapan et al., 2021). Transferring sensitive materials from glove boxes to a measurement system without environmental control is another major obstacle, requiring a sealed transfer system or the use of encapsulation techniques (Ahangar and Farmanzadeh, 2023), which adds complexity and risk of contamination or damage.

Recently, the metal-assisted mechanical exfoliation technique has emerged as a feasible solution for large-area 2D material production (Wu et al., 2024a; Petrini et al., 2024; Grubišić-Čabo et al., 2023; Liu et al., 2020). By exploiting the stronger adhesion between the metals and the outermost layer of bulk layered crystals, this technique can produce monolayers on a millimeter–or even centimeter–scale by pressing a tape containing a bulk crystal on clean, smooth metal substrates, such as gold (Liu et al., 2020). The resulting large lateral size is crucial for device fabrication and characterization, facilitating standard photolithography, scalable manufacturing, and high-quality 2D heterostructure integration, while also meeting the dimensional requirements of techniques like X-ray photoelectron spectroscopy (XPS) for reliable material analysis. However, this method is typically performed under ambient conditions, making it unsuitable for air-sensitive materials. Moreover, this method is incompatible with surface techniques that require *in situ* surface cleaning.

Here, we employed an ultra-high vacuum (UHV) exfoliation method (Grubišić-Čabo et al., 2023) to prepare large-area monolayers of TMDC films. While having the same advantages as ME over bottom-up synthesis techniques, our method also performs better for certain applications over liquid-phase exfoliation. Liquid phase exfoliation produces exfoliated monolayers that typically have lower crystalline quality, higher defect density, and smaller lateral dimensions, albeit in a high quantity, and our method provides better control of the sheet size and thickness, provided the substrate is suitable for this approach (Paton et al., 2014). The comparison of various exfoliation methods can be found in the Supplementary Table S2. Using the aforementioned UHV exfoliation approach we successfully produced near-millimeter-scale monolayers of WS_2 and WSe_2 on metal substrates. To isolate the influence of a chalcogen's affinity for a specific substrate material, both Ag and Au substrates were employed. Low-energy electron diffraction (LEED) was used to explore existence of potential preferred angle between the layered film and the metal substrates, while optical microscopy was used to study the exfoliation yield of monolayer WSe_2 and WS_2. Atomic force microscopy (AFM) was employed to verify the thickness of exfoliated flakes. Finally, XPS and X-ray diffraction were used to investigate chemical bonding and substrate quality following UHV exfoliation. Our findings demonstrate the feasibility of the UHV exfoliation method for producing high-quality, large-area monolayer TMDCs, as the nearly millimeter-scale exfoliated flakes retain their crystallinity and are well-suited for *in situ* surface studies. Importantly, the size of the flakes correlates with the quality of the parent crystals, highlighting the potential of this technique for advancing scalable, high-quality 2D material production.

2 Materials and methods

2.1 Materials

WS_2 and WSe_2 bulk crystals were purchased from HQ Graphene, with a lateral size of ≈ 5 mm. The bulk crystals were cut to suitable dimensions to fit customized holders and mounted using vacuum-compatible silver epoxy (EPO-TEK). Prior to loading into the load-lock chamber, the surface of each crystal was tape-cleaved to ensure flatness of the surface. Following this, a pre-prepared adhesive tape (Lyreco, INVISIBLE TAPE) was attached to the top of the crystal for subsequent mechanical cleavage under UHV conditions.

Ag (111)/mica and Au (111)/mica (Georg-Albert-PVD) substrates were cut to the appropriate size and fixed to a flag style sample plate by welded tantalum strips. The Au and Ag substrates were cleaned using repeated cycles of Ar^+ sputtering (45 min at 1.0×10^{-6} mbar and 1.5 kV) and annealing (30 min at 600 K).

2.2 Characterization techniques

2.2.1 Low-energy electron diffraction

LEED measurements (SPECS ErLEED 1000A) with a 1 mm spot size were performed at room temperature under a pressure of $\approx 5 \times 10^{-10}$ mbar, using electron energy of 125 eV for all samples. LEED was used to verify the cleanliness of the Au (111) and Ag (111) substrates following the cleaning procedure (prior to exfoliation) and to confirm the success of exfoliation after the exfoliation process.

2.2.2 Optical microscopy

Monolayers of exfoliated materials were identified using optical contrast technique. Optical images were acquired with an Olympus microscope and processed using ImageJ software to analyze regions corresponding to monolayer contrast. The images were split into red, green and blue (RGB) channels, with the red channel selected for analysis due to its excellent contrast. ImageJ threshold routines were applied to identify flakes and calculate monolayer areas as well as lateral sizes, represented by the maximum Feret diameter. Statistical analysis of the size distributions was performed by fitting the data to a log-normal distribution.

2.2.3 Atomic force microscopy

AFM was conducted under ambient conditions with Dimension FastScan Bruker and Cypher S AFM (Asylum Research) microscopes using the AC160-TSA tip. The measurements were performed in tapping mode. The AFM was calibrated using a standard calibration sample prior to the experiments. AFM data analysis was carried out using the Gwyddion software package.

The Kelvin probe force microscopy (KPFM) measurements were performed on an Asylum Research Cypher ES atomic force microscope using Co/Cr-coated Sb-doped Si tips from Bruker (MESP-RC-V2, k = 5 N/m, f_0 = 150 kHz). The surface potential measurements were acquired in non-contact mode, following a two-pass protocol: In the first pass, the surface topography is recorded in standard AC tapping mode, while in the second pass the electrostatic tip-sample interaction is measured at a constant lift height of 40 nm. During the second pass, the cantilever is electrically excited by an AC voltage with an amplitude of 800 mV and a frequency of 147 kHz. A DC bias is applied to the tip during the second pass to minimize the electrostatic tip-sample interaction via the closed-loop feedback and is used to obtain the surface potential.

2.2.4 Scanning electron microscopy

Scanning electron microscopy (SEM) characterization was performed using a FEI NovaNano NanoSEM 650 instrument operated at an acceleration voltage of 10 kV in secondary electrons mode. The sample was supported to a metal stub using conductive double-sided carbon tape to hold the sample securely.

2.2.5 X-ray photoelectron spectroscopy

XPS measurements of the TMDC/metal samples were performed using an SSX-100 (Surface Science Instruments) spectrometer equipped with a monochromatic Al Kα X-ray source ($h\nu$ = 1486.6 eV). The measurement chamber pressure was maintained at 1×10^{-9} mbar during data acquisition, with a photoelectron take-off angle of 37° relative to the surface normal. The analyzed area had a diameter of 1 mm^2 and the energy resolution was 1.6 eV. The binding energy (BE) values were reported with an accuracy of 0.1 eV and referenced to the C 1*s* core level of adventitious carbon at 284.91 eV (Biesinger, 2022). All XPS spectra were analyzed using the least-squares curve-fitting program Winspec (developed at LISE, University of Namur, Belgium). Spectral fitting included Shirley (for W 4*f*) and liner background subtraction (for S 2*p* & Se 3*p*). Because the S 2*p* and Se 3*p* peaks lie on the intense Au W 4*f* background, a linear background subtraction was deemed sufficient for accurately isolating the peak signals (Castle et al., 2000). The peak profiles were modeled as a convolution of Gaussian and Lorentzian functions using the minimum number of peaks necessary to reflect the chemical structure of the sample, while accounting for experimental resolution. The uncertainty in the peak intensity determination was within 2% for all of the core-level spectra, with measurements taken at two points for each sample.

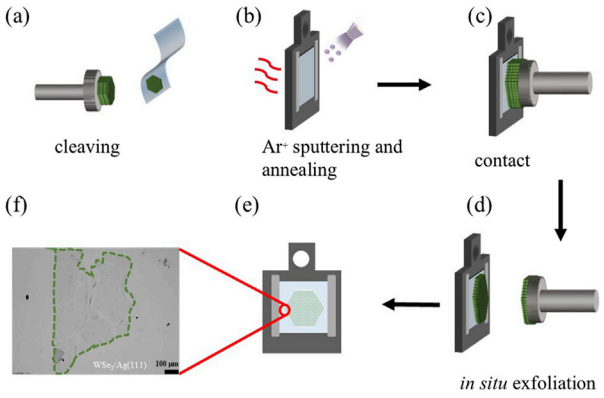

FIGURE 1
A schematic of the kinetic *in situ* single layer synthesis (KISS) exfoliation process: **(a)** preparation of an ultra-flat, clean WSe_2 surface. **(b)** sputtering and annealing of the Ag (111) substrate to achieve an atomically clean and flat surface. Freshly prepared surfaces are brought into contact **(c)**, followed by careful separation **(d)** to enable *in situ* exfoliation of the 2D material onto the substrate **(e)**. This process results in deposition of a high-quality, large-area monolayer 2D material, verified by optical microscopy, with single-layer WSe_2 successfully transferred onto the Ag (111) substrate **(f)**.

3 Results and discussion

3.1 Exfoliation of monolayers in UHV

Samples were prepared using the kinetic *in situ* single-layer synthesis (KISS) method, as illustrated in Figure 1 for the case of WSe_2 on Ag (111). The KISS exfoliation process, along with the pre-treatment of bulk crystals and metallic substrates (detailed in the Materials and Methods section), was conducted under UHV conditions maintaining a pressure better than 1×10^{-9} mbar. Figure 1a depicts preparation of a clean bulk surface of WSe_2 by adhesive tape cleaving in UHV. To ensure that the surface is as clean as possible, this step is performed shortly before the KISS exfoliation takes place. Figure 1b illustrates the substrate preparation process, which involved multiple cycles of Ar^+ sputtering and annealing to remove surface impurities and moisture (Mohamedi et al., 2022). After three cleaning cycles, the substrate was naturally cooled to room temperature. At this point, KISS exfoliation was performed by bringing a freshly cleaved WSe_2 bulk crystal into contact with the substrate, Figure 1c, followed by the controlled separation of bulk crystal from the substrate, Figure 1d. Due to the strong adhesion between the metallic substrate and TMDC (Wu et al., 2024a), in this case WSe_2, the topmost layer–or, in some cases, a few layers–is exfoliated onto the substrate, Figure 1e. An example of KISS-exfoliated monolayer (ML) WSe_2 on Ag (111) is shown in Figure 1f, with the ML flake (outlined in green) having a lateral

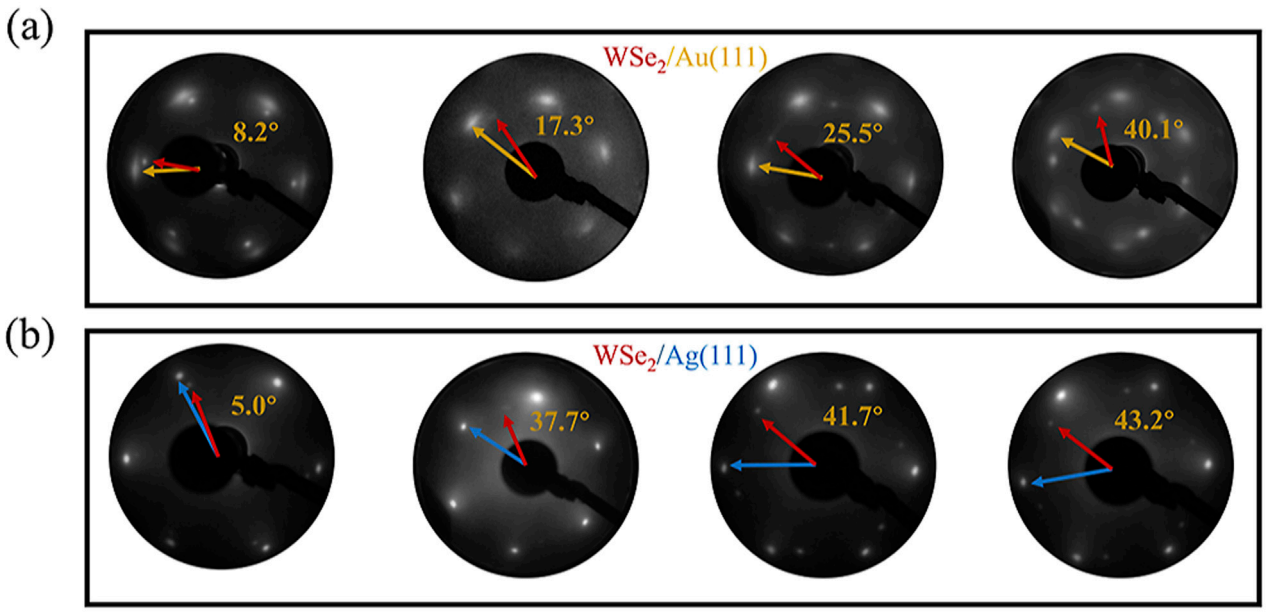

FIGURE 2
Low-energy electron diffraction (LEED) analysis of the rotational alignment between the exfoliated 2D material and the substrate: **(a)** LEED images of WSe_2 on Au (111); **(b)** LEED images of WSe_2 on Ag (111). All images were obtained with an electron energy of 125 eV. The red arrow points to the diffraction pattern of WSe_2, and the yellow and blue arrows indicate the diffraction features of Au and Ag, respectively. No preferred rotational alignment is observed on either substrate.

size of approximately 500 μm. Typically, when crystal was significantly smaller than the substrate, exfoliation was performed at several distinct locations on the substrate surface to increase the coverage. Using this method, monolayers were obtained on nearly all substrates, with the primary difference being their lateral sizes.

3.2 Surface morphology and structure

3.2.1 Angular alignment with the substrate

Following exfoliation procedure, *in situ* characterization was conducted using the LEED system mounted on the same UHV chamber. As shown in Figure 2, LEED patterns were obtained for four individual flakes exfoliated onto Au (111), Figure 2a, and Ag (111) substrates, Figure 2b. All pattern exhibited distinct nested hexagonal diffraction patterns, consistent with the hexagonal crystalline lattices of WSe_2, Ag (111) and Au (111). The outer hexagons in Figure 2 originate from the substrates (Au or Ag), while the inner hexagons come from WSe_2. The presence of both hexagonal patterns confirms the successful exfoliation of WSe_2 (Grubišić-Čabo et al., 2023). Notably, the sharper and brighter diffraction spots observed in WS_2 compared to WSe_2 can be attributed to its higher lattice phonon frequency (Wu et al., 2024b), which inherently corresponds to smaller amplitudes of atomic thermal vibrations and results in reduced attenuation of elastic scattering intensity (Chuang et al., 2022). Incidentally, the diffraction spots from the Au (111) substrate are significantly broader than those from the Ag (111) substrate. This broadening, also observed for WS_2/Au (111) samples (see Supplementary Figure S1A), suggests that the coherently diffracting domains are smaller in the case of Au (111) thin films grown on mica than in the Ag (111) ones. Moreover, one also notices that the Au (111) spots are slightly elongated, contrary to the Ag (111) spots which are round. This points to a slight misalignment between Au (111) grains and higher step density (Man et al., 2016; Haider et al., 2024).

TABLE 1 Summary of twist angles between TMDCs and substrates based on LEED images of WS_2/Au, WS_2/Ag, WSe_2/Au, and WSe_2/Ag. In each case four individual samples were examined. No preferred orientation was observed for any of the samples.

	Sample 1	Sample 2	Sample 3	Sample 4
WS_2/Ag (111)	4.4°	9.2°	28.1°	34.4°
WS_2/Au (111)	8.7°	20.2°	47.1°	56.8°
WSe_2/Ag (111)	5.0°	37.7°	41.7°	43.2°
WSe_2/Au (111)	8.2°	17.3°	25.5°	40.1°

Epitaxially grown 2D materials typically exhibit preferred stacking orientation relative to the substrate they are grown on (Choudhury et al., 2020). However, KISS exfoliation does not favor a specific stacking orientation alignment between the exfoliated 2D materials and its substrates, as seen from the LEED patterns. Table 1 summarizes the twist angles derived from Figure 2 and Supplementary Figure S1, showing significant angular variations between the TMDC flakes and the substrates, with angles randomly distributed between 0° and 60°. Furthermore, lattice matching between the metal substrate and the TMDC seems to have no effect on the exfoliation process. In other words, we can exclude

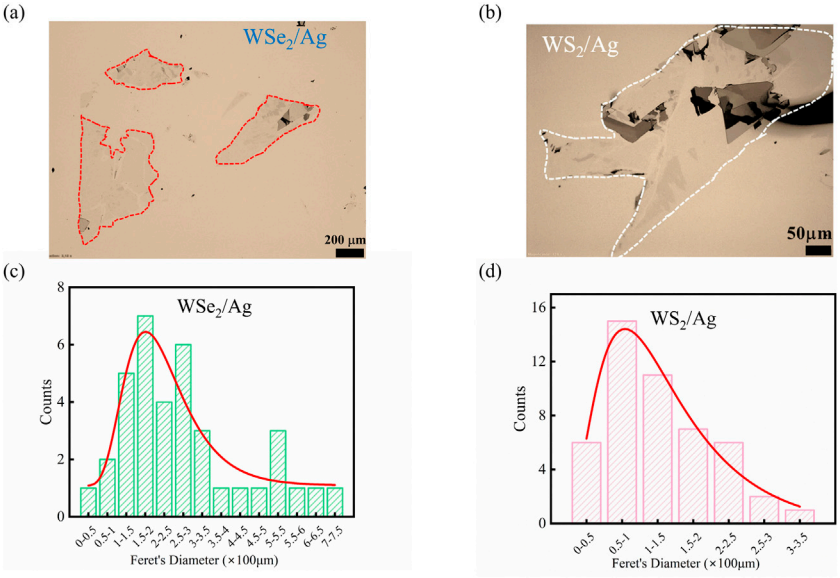

FIGURE 3
Optical microscopy characterization of exfoliated flake size distribution: **(a)** and **(b)** are representative optical images of WSe_2/Ag (111) and WS_2/Ag (111), respectively. **(c)** Distribution of flake lateral size (maximum Feret diameter) of the optical image for four WSe_2/Ag (111) samples. Optical images of the other samples are shown in Supplementary Figure S3. **(d)** Distribution of flake lateral size for four WS_2/Ag (111) samples. Optical images of the other samples are shown in Supplementary Figure S3. Histograms showing the counts of different lateral sizes of flakes are fitted using a log-normal distribution, visualized by the solid red line. The p-values are all less than 0.05, indicating that the log-normal distribution is suitable.

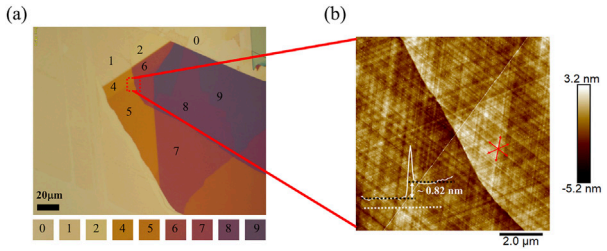

FIGURE 4
Thickness characterization based on color variations observed in the optical microscopy image: **(a)** optical image of the WS_2/Ag (111). Different layers correspond to different colors and are indicated by numbers 0–9, where 0 represents bare Ag and nine corresponds to nine layers of WS_2. **(b)** AFM measurements conducted within the red square outlined in **(a)**. The white solid line represents the step height (≈ 0.82 nm) along the dashed line, confirming a single-layer thickness difference between adjacent layers.

that grains in the parent crystal of Au (Ag) with a specific orientation with respect to the TMDC substrate attach more easily (Haider et al., 2024).

3.2.2 Role of chalcogen atom

The presence of different chalcogen atoms influences various intrinsic properties of TMDCs (Huang et al., 2020), but their influence on KISS exfoliation trends remains unclear. Figure 3 presents the exfoliation results of WS_2 and WSe_2 on Ag (111) substrates, as observed by optical microscopy. Despite using the same type of substrate and proceeding with the exfoliation in an identical manner, differences in exfoliation yield between the two materials are clearly evident. For WSe_2/Ag (111) sample, shown in Figure 3a, large and crack-free monolayer flakes were consistently produced, up to a maximum lateral size of 750 μm. Only a few flakes exhibited thicknesses exceeding that of a monolayer, and in some instances, minor bulk structures were observed at the edges of flakes. In contrast, WS_2/Ag (111), shown in Figure 3b, displayed a more fragmented morphology with smaller flake size and a significant presence of few-layer and bulk structures. This fragmentation and presence of thicker structures makes it challenging to isolate individual monolayer flakes suitable for further characterization. To rule out substrate effects, the same protocol was applied to WS_2/Au (111) and WSe_2/Au (111) samples (shown in Supplementary Figure S2). The results confirmed that WS_2 consistently exhibited greater fragmentation, further emphasizing the role of the chalcogen elements in facilitating exfoliation.

To quantitatively evaluate the yield of monolayer flakes, we measured and analyzed the size distribution of flakes from four different samples. Given the predominantly irregular morphology of the exfoliated flakes, the Feret diameter was used to determine their lateral dimensions (Petrini et al., 2024; Kröner and Hirsch, 2020). Using ImageJ software, the Feret diameters were extracted by manually applying an appropriate threshold, which meant setting the contrast range manually, where pixels above the threshold are considered as TMDC, while those below are attributed to the substrate (Schneider et al., 2012; Puebla et al., 2022). As shown in Figure 3c, the statistical size distribution for the four WSe_2/Ag (111) samples reveals that most flakes fall within the 200-250 μm range, with the largest lateral dimension reaching up to 750 μm. In contrast, the statistical analysis for the four WS_2/Ag (111) samples, Figure 3d, indicates that the flakes are primarily within the 100-150 μm range, with a maximum size of 350 μm, and display a higher degree of

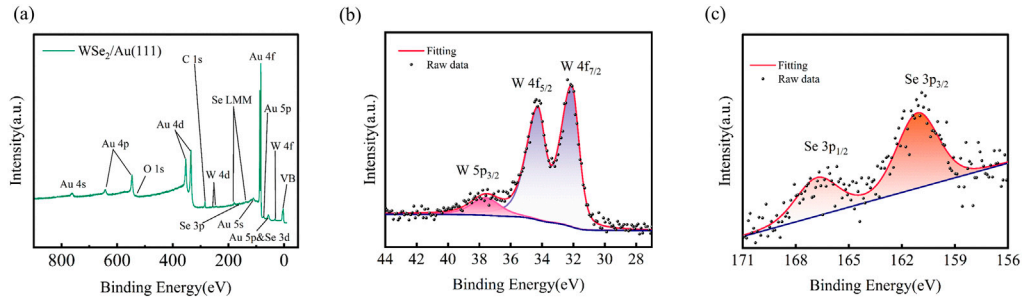

FIGURE 5
X-ray photoelectron spectroscopy (XPS) characterization of WSe_2/Au (111): **(a)** Wide scan of WSe_2/Au (111) showing the expected Au, W and Se peaks. The presence of C and O peaks suggests potential contamination from adsorption during the transfer process which was performed in air, or insufficient annealing prior to measurement. Detailed scans of the **(b)** W 4*f* and **(c)** Se 3*p* core level regions (dots) with their corresponding fits (continuous line). No signs of oxidation are observed for either W or Se. The XPS spectra of W were background-subtracted using the Shirley background, while from the Se spectra a linear background was subtracted because it sits on the intense Au 4*f* background.

fragmentation. The same analysis for WSe_2 and WS_2 on Au (111) can be found in the Supplementary information, Supplementary Figures S2C, F and is in agreement with the results on Ag (111).

The larger dimensions of WSe_2 flakes, the absence of cracks in the transferred WSe_2 flakes and higher overall coverage of the substrate indicate a more stable and robust interaction with the noble metal during the KISS process. This behavior can be attributed to the larger atomic radius and higher polarization of Se atoms, which result in stronger van der Waals interaction between the WSe_2 flakes and the substrate (Huang et al., 2020). Additionally, the lower electronegativity of Se facilitates the charge transfer between WSe_2 and the substrate, thereby enhancing the charge coupling effect at the interface (Xing et al., 2020). It is worth noting that these outcomes may also be influenced by the quality of the parent crystals, as the bulk WSe_2 crystal appeared to have higher quality with fewer bulk defects, Supplementary Figure S6.

3.2.3 Surface morphology

To investigate the flake thickness, optical microscopy, Figure 4a, and AFM, Figure 4b, were used. The distinct color distribution observed in the optical images clearly indicates regions of varying thickness (Puebla et al., 2022). The step profile analysis showed that the monolayer thickness is approximately 0.82 nm, which is slightly larger than previously reported values for monolayer WS_2 (Chuang et al., 2022). This difference in height can be attributed to AFM instrumental offset, as well as the presence of adventitious carbon, impurities or moisture on the TMDC surface from exposure to air before and during AFM measurements (Fang et al., 2012; Gammelgaard et al., 2021; Rasche et al., 2022). By combining AFM measurements and optical microscopy data, the color of the flake can be correlated with its thickness, as shown in Figure 4a, allowing for faster identification of the layer number, similar to what has been done for mechanically exfoliated 2D materials on SiO_2/Si (Puebla et al., 2022).

In the AFM topography, a distinct regular pattern can also be observed, marked with red arrows in Figure 4b, which appears to originate from the underlying substrate. The angle between the lines in the pattern is exactly 60°, and the pattern arises from the local reconstruction of surface steps along the symmetric crystallographic directions of the Ag (111) surface after annealing, resulting in the formation of periodic stripes (Sweetman et al., 2013).

3.3 Chemical composition and interfacial properties

We performed XPS measurements to better understand the interaction between TMDCs and metal surfaces. WSe_2 and WS_2 were measured on Ag (111) and Au (111) substrates, respectively. Figure 5a presents the wide scan spectrum of WSe_2/Au (111), which is used to identify the elements present on the surface. The characteristic peaks corresponding to the W 4*f*, W 4*d*, Se 3*d*, and Se 3*p* orbitals confirm the presence of WSe_2, and demonstrate that KISS exfoliated flakes are large enough to be located and measured with a 1 mm^2 beam. The C 1*s* peak indicates the presence of adventitious carbon, likely resulting from the transfer in air from the exfoliation chamber to the XPS chamber (Petrini et al., 2024).

Figures 5b,c show detailed spectra for W 4*f* and Se 3*p*. The asymmetry observed in the W 4*f* peak is attributed to shake-up events, promoting conduction electrons from below to above the Fermi level. The Se $3p_{1/2}$ and Se 3 $p_{3/2}$ lines are located at binding energies of 161.21 eV and 167.21 eV, respectively. The W 4 $f_{7/2}$ and W $4f_{5/2}$ lines are located at binding energies of 31.6 eV and 33.8 eV, respectively. The binding energies of W 4*f* for WSe_2 and WS_2 on Au and Ag substrates, as summarized in Supplementary Table S1, show slight variations in different samples, but remain consistent with previous reports (Wu et al., 2022; Shen et al., 2022; Bignardi et al., 2019; Dendzik et al., 2017). Since no components related to WO_x can be seen in the W 4*f* spectra, nor components related to oxidized selenium (162 eV (Tong et al., 2016)) and sulfur (168.8 eV (Park et al., 2024)) are found, we conclude that KISS exfoliated WSe_2 and WS_2 layers are air-stable, similar to MBE grown samples (Beyer et al., 2019; Xia et al., 2023). Although changes in XPS binding energy suggest some degree of charge transfer, no clear evidence of Se (S)-Au (Ag) covalent bonding was observed in the XPS spectra. This potential charge transfer was further examined through KPFM measurements (Supplementary Figures S8) on the WS_2/Ag sample, which revealed that the surface potential of Ag is 55 mV higher than that of WS_2. This observation confirms charge redistribution at the interface, consistent with previous

reports (Huang et al., 2020; Freedy and McDonnell, 2020). Similar findings by Velicky et al. (2018) suggest that the observed charge transfer primarily contributes to physical adsorption, while the interface remains dominated by van der Waals interactions.

Since KISS exfoliation involves the mechanical contact of a bulk crystal with another solid surface, it is essential to assess whether the process induces any damage to the substrate. To evaluate the impact of exfoliation on the substrate, we measured the (111) Bragg reflection of a single-crystal silver substrate in a near-backscattering geometry (see Section 4 in SI), which is sensitive to deformation of the substrate lattice. The measurement was performed with a focused beam aligned to a WSe_2 flake after KISS procedures. The width of the Ag (111) reflectivity curve, shown in Supplementary Figures S5D, was determined to be 0.95 eV, which is identical to the intrinsic width of the Ag (111) reflection convoluted with the energy width of the optics, indicating that the exfoliation process of WSe_2 has a negligible effect on the crystallinity of the substrate. Furthermore, as shown in Supplementary Figures S7, the SEM images reveal that the substrate remains structurally intact, with no visible cracks or fractures, and the surface remains smooth and uniform, further confirming that the KISS methods does not damage the substrate. This finding underscores the suitability of KISS exfoliation for preparing high-quality monolayer TMDCs while preserving the substrate's properties for subsequent characterization and applications.

4 Conclusion

The KISS exfoliation method has proven to be a reliable method for producing high-quality large-area monolayers of WS_2 and WSe_2, on metallic substrates in ultra-high vacuum. Notably, exfoliation of WSe_2 yielded crack-free flakes with larger lateral dimensions and a higher overall coverage of the substrate than the exfoliation of WS_2, presumably due to the higher quality of WSe_2 bulk crystal and to selenium's advantageous atomic properties, including its larger radius, higher polarization, and lower electronegativity. By combining optical microscopy and atomic force microscopy, we demonstrate that optical microscopy is a practical method for layer identification based on color contrast. Structural analysis using low-energy electron diffraction revealed that there is no preferred angle between the substrates and the two-dimensional transition metal dichalcogenides, implying that lattice matching between the substrate and transition metal dichalcogenide seems to have no effect on the exfoliation process, and thus one can exclude that grains in the parent crystal with a specific orientation with respect to the substrate attach more easily. Chemical analysis by X-ray photoelectron spectroscopy verified the air-stability of the exfoliated films, and no signs of covalent bonding between the substrate and transition metal dichalcogenides were found, with only mild charge transfer effects observed. This suggests that while interaction between the substrate and the topmost transition metal dichalcogenide layer is stronger than the transition metal dichalcogenide interlayer bonds, it is not of covalent nature. Furthermore, X-ray diffraction confirmed that the exfoliation process has no impact on the crystalline quality of the metallic substrate, demonstrating the method's non-destructive nature. These results validate kinetic *in situ* single-layer synthesis method as an excellent technique for fabricating high-quality, large-area crack-free monolayer transition metal dichalcogenides on metallic substrates without substrate degradation.

Data availability statement

The datasets presented in this study can be found in online repositories. The names of the repository/repositories and accession number(s) can be found below: Zenodo: https://doi.org/10.5281/zenodo.14537302.

Author contributions

ZD: Conceptualization, Formal Analysis, Investigation, Visualization, Writing – original draft, Writing – review and editing. RSE: Formal Analysis, Investigation, Writing – review and editing. GF: Investigation, Writing – review and editing. MV: Investigation, Writing – review and editing. DG: Investigation, Writing – review and editing. MFS: Writing – original draft, Writing – review and editing, Investigation, Data curation, Formal analysis. YZ: Writing – original draft, Writing – review and editing, Investigation, Data curation. PR: Resources, Supervision, Writing – review and editing. AG-C: Conceptualization, Funding acquisition, Investigation, Project administration, Supervision, Writing – original draft, Writing – review and editing.

Funding

The author(s) declare that financial support was received for the research and/or publication of this article. This work was supported by the Zernike Institute for Advanced Materials. AG-C and PR acknowledge the research program "Materials for the Quantum Age" (QuMat) for financial support. This program (registration number 024.005.006) is part of the Gravitation program financed by the Dutch Ministry of Education, Culture and Science (OCW). ZD acknowledges the fellowship from the Chinese Scholarship Council (No. 202206750016).

Acknowledgments

AG-C acknowledges financial support of the Zernike Institute for Advanced Materials. AG-C and PR acknowledge the research program "Materials for the Quantum Age" (QuMat) for financial support. This program (registration number 024.005.006) is part of the Gravitation program financed by the Dutch Ministry of Education, Culture and Science (OCW). ZD acknowledges the fellowship from the Chinese Scholarship Council (No.202206750016). The authors would like to thank Diamond Light Source for beamtime (proposal SI35796) and the staff of beamline I09, Deepnarayan Biswas and Tien-Lin Lee, for their assistance with experiments and data collection.

Conflict of interest

The authors declare that the research was conducted in the absence of any commercial or financial relationships that could be construed as a potential conflict of interest.

Generative AI statement

The author(s) declare that no Gen AI was used in the creation of this manuscript.

Publisher's note

All claims expressed in this article are solely those of the authors and do not necessarily represent those of their affiliated organizations, or those of the publisher, the editors and the reviewers. Any product that may be evaluated in this article, or claim that may be made by its manufacturer, is not guaranteed or endorsed by the publisher.

Supplementary material

The Supplementary Material for this article can be found online at: https://www.frontiersin.org/articles/10.3389/fnano.2025.1553976/full#supplementary-material

References

Ahangar, R. M., and Farmanzadeh, D. (2023). Effects of hexagonal boron nitride encapsulation on the electronic properties of Cu, Li, and O-doped black phosphorus monolayer. *Phys. B Condens. Matter* 660, 414880. doi:10.1016/j.physb.2023.414880

Beyer, H., Rohde, G., Grubišić Čabo, A., Stange, A., Jacobsen, T., Bignardi, L., et al. (2019). 80% Valley Polarization of free carriers in singly oriented single-layer WS_2 on Au (111). *Phys. Rev. Lett.* 123, 236802. doi:10.1103/physrevlett.123.236802

Biesinger, M. C. (2022). Accessing the robustness of adventitious carbon for charge referencing (correction) purposes in XPS analysis: insights from a multi-user facility data review. *Appl. Surf. Sci.* 597, 153681. doi:10.1016/j.apsusc.2022.153681

Bignardi, L., Lizzit, D., Bana, H., Travaglia, E., Lacovig, P., Sanders, C. E., et al. (2019). Growth and structure of singly oriented single-layer tungsten disulfide on Au (111). *Phys. Rev. Mater.* 3, 014003. doi:10.1103/physrevmaterials.3.014003

Buapan, K., Somphonsane, R., Chiawchan, T., and Ramamoorthy, H. (2021). Versatile, low-cost, and portable 2D material transfer setup with a facile and highly efficient DIY inert-atmosphere glove compartment option. *ACS Omega* 6, 17952–17964. doi:10.1021/acsomega.1c01582

Carré, E., Sponza, L., Lusson, A., Stenger, I., Roux, S., Fossard, F., et al. (2024). Luminescence of black phosphorus films: exfoliation-induced defects and confined excitations. *Phys. Rev. B* 109, 035424. doi:10.1103/physrevb.109.035424

Castle, J., Chapman-Kpodo, H., Proctor, A., and Salvi, A. M. (2000). Curve-fitting in XPS using extrinsic and intrinsic background structure. *J. Electron Spectrosc. Relat. Phenom.* 106, 65–80. doi:10.1016/s0368-2048(99)00089-4

Choudhury, T. H., Zhang, X., Al Balushi, Z. Y., Chubarov, M., and Redwing, J. M. (2020). Epitaxial growth of two-dimensional layered transition metal dichalcogenides. *Annu. Rev. Mater. Res.* 50, 155–177. doi:10.1146/annurev-matsci-090519-113456

Chuang, H.-J., Phillips, M., McCreary, K. M., Wickramaratne, D., Rosenberger, M. R., Oleshko, V. P., et al. (2022). Emergent moiré phonons due to zone folding in WSe_2–WS_2 Van Der Waals Heterostructures. *ACS Nano* 16, 16260–16270. doi:10.1021/acsnano.2c05204

Dendzik, M., Bruix, A., Michiardi, M., Ngankeu, A. S., Bianchi, M., Miwa, J. A., et al. (2017). Substrate-induced semiconductor-to-metal transition in monolayer WS_2. *Phys. Rev. B* 96, 235440. doi:10.1103/physrevb.96.235440

Ellis, J. K., Lucero, M. J., and Scuseria, G. E. (2011). The indirect to direct band gap transition in multilayered MoS_2 as predicted by screened hybrid density functional theory. *Appl. Phys. Lett.* 99. doi:10.1063/1.3672219

Fang, H., Chuang, S., Chang, T. C., Takei, K., Takahashi, T., and Javey, A. (2012). High-performance single layered WSe_2 p-FETs with chemically doped contacts. *Nano Lett.* 12, 3788–3792. doi:10.1021/nl301702r

Feraco, G., De Luca, O., Przybysz, P., Jafari, H., Zheliuk, O., Wang, Y., et al. (2024). Nano-ARPES investigation of structural relaxation in small angle twisted bilayer tungsten disulfide. *Phys. Rev. Mater.* 8, 124004. doi:10.1103/physrevmaterials.8.124004

Freedy, K. M., and McDonnell, S. J. (2020). Contacts for molybdenum disulfide: interface chemistry and thermal stability. *Materials* 13, 693. doi:10.3390/ma13030693

Gammelgaard, L., Whelan, P. R., Booth, T. J., and Bøggild, P. (2021). Long-term stability and tree-ring oxidation of WSe_2 using phase-contrast AFM. *Nanoscale* 13, 19238–19246. doi:10.1039/d1nr05413a

Georgiou, T., Jalil, R., Belle, B. D., Britnell, L., Gorbachev, R. V., Morozov, S. V., et al. (2013). Vertical field-effect transistor based on graphene–WS_2 heterostructures for flexible and transparent electronics. *Nat. Nanotechnol.* 8, 100–103. doi:10.1038/nnano.2012.224

Grubišić-Čabo, A., Michiardi, M., Sanders, C. E., Bianchi, M., Curcio, D., Phuyal, D., et al. (2023). *In situ* exfoliation method of large-area 2D materials. *Adv. Sci.* 10, 2301243. doi:10.1002/advs.202301243

Haider, G., Gastaldo, M., Karim, B., Plsek, J., Varade, V., Volochanskyi, O., et al. (2024). Highly efficient bulk-crystal-sized exfoliation of 2D materials under ultrahigh vacuum. *ACS Appl. Electron. Mater.* 6, 2301–2308. doi:10.1021/acsaelm.3c01824

Huang, Y., Pan, Y.-H., Yang, R., Bao, L.-H., Meng, L., Luo, H.-L., et al. (2020). Universal mechanical exfoliation of large-area 2D crystals. *Nat. Commun.* 11, 2453. doi:10.1038/s41467-020-16266-w

Islam, M. A., Serles, P., Kumral, B., Demingos, P. G., Qureshi, T., Meiyazhagan, A., et al. (2022). Exfoliation mechanisms of 2D materials and their applications. *Appl. Phys. Rev.* 9. doi:10.1063/5.0090717

Kezilebieke, S., Huda, M. N., Dreher, P., Manninen, I., Zhou, Y., Sainio, J., et al. (2020). Electronic and magnetic characterization of epitaxial VSe_2 monolayers on superconducting $NbSe_2$. *Commun. Phys.* 3, 116. doi:10.1038/s42005-020-0377-4

Kim, H.-U., Kanade, V., Kim, M., Kim, K. S., An, B.-S., Seok, H., et al. (2020). Wafer-scale and low-temperature growth of 1T-WS_2 film for efficient and stable hydrogen evolution reaction. *Small* 16, 1905000. doi:10.1002/smll.201905000

Kröner, A., and Hirsch, T. (2020). Current trends in the optical characterization of two-dimensional carbon nanomaterials. *Front. Chem.* 7, 927. doi:10.3389/fchem.2019.00927

Li, L., Li, S., Wang, W., Zhang, J., Sun, Y., Deng, Q., et al. (2024). Adaptative machine vision with microsecond-level accurate perception beyond human retina. *Nat. Commun.* 15, 6261. doi:10.1038/s41467-024-50488-6

Liu, F., Wu, W., Bai, Y., Chae, S. H., Li, Q., Wang, J., et al. (2020). Disassembling 2D van der Waals crystals into macroscopic monolayers and reassembling into artificial lattices. *Science* 367, 903–906. doi:10.1126/science.aba1416

Man, M. K., Deckoff-Jones, S., Winchester, A., Shi, G., Gupta, G., Mohite, A. D., et al. (2016). Protecting the properties of monolayer MoS_2 on silicon based substrates with an atomically thin buffer. *Sci. Rep.* 6, 20890. doi:10.1038/srep20890

Mohamedi, M., Challali, F., Touam, T., Mendil, D., Ouhenia, S., Souici, A., et al. (2022). Role of substrate and annealing on microstructural, optoelectronic and luminescence properties of RF magnetron sputtered AZO thin films in confocal configuration. *J. Luminescence* 244, 118739. doi:10.1016/j.jlumin.2022.118739

Park, J., Cho, I., Jeon, H., Lee, Y., Zhang, J., Lee, D., et al. (2024). Conversion of layered WS_2 crystals into mixed-domain electrochemical catalysts by plasma-assisted surface reconstruction. *Adv. Mater.* 36, 2314031. doi:10.1002/adma.202314031

Paton, K. R., Varrla, E., Backes, C., Smith, R. J., Khan, U., O'Neill, A., et al. (2014). Scalable production of large quantities of defect-free few-layer graphene by shear exfoliation in liquids. *Nat. Mater.* 13, 624–630. doi:10.1038/nmat3944

Petrini, N., Peci, E., Curreli, N., Spotorno, E., Kazemi Tofighi, N., Magnozzi, M., et al. (2024). Optimizing gold-assisted exfoliation of layered transition metal dichalcogenides with (3-aminopropyl) triethoxysilane (APTES): a promising approach for large-area monolayers. *Adv. Opt. Mater.* 12, 2303228. doi:10.1002/adom.202303228

Pirker, L., Honolka, J., VelickÝ, M., and Frank, O. (2024). When 2D materials meet metals. *2D Mater.* 11, 022003. doi:10.1088/2053-1583/ad286b

Puebla, S., Li, H., Zhang, H., and Castellanos-Gomez, A. (2022). Apparent colors of 2D materials. *Adv. Photonics Res.* 3, 2100221. doi:10.1002/adpr.202100221

Rasche, B., Brunner, J., Schramm, T., Ghimire, M. P., Nitzsche, U., Buchner, B., et al. (2022). Determination of cleavage energy and efficient nanostructuring of layered materials by atomic force microscopy. *Nano Lett.* 22, 3550–3556. doi:10.1021/acs.nanolett.1c04868

Schneider, C. A., Rasband, W. S., and Eliceiri, K. W. (2012). NIH Image to ImageJ: 25 years of image analysis. *Nat. Methods* 9, 671–675. doi:10.1038/nmeth.2089

Schütze, A., Schädlich, P., Seyller, T., and Göhler, F. (2024). Exploring metal-organic molecular beam epitaxy as an alternative pathway towards 2D transition metal dichalcogenides WSe_2 and WS_2. *Small Struct.*, 2400306. doi:10.1002/sstr.202400306

Shen, P., Li, X., Luo, Y., Guo, Y., Zhao, X., and Chu, K. (2022). High-efficiency N_2 electroreduction enabled by Se-vacancy-rich WSe_{2-x} in water-in-salt electrolytes. *ACS Nano* 16, 7915–7925. doi:10.1021/acsnano.2c00596

Sweetman, A., Stannard, A., Sugimoto, Y., Abe, M., Morita, S., and Moriarty, P. (2013). Simultaneous noncontact AFM and STM of Ag: Si (111)-(3 × 3) R 30°. *Phys. Rev.* 87, 075310. doi:10.1103/physrevb.87.075310

Tong, Y., Jiang, T., Bendounan, A., Nicolas, F., Kubsky, S., and Esaulov, V. A. (2016). Selenium, benzeneselenol, and selenophene interaction with cu (100). *J. Phys. Chem. C* 120, 21486–21495. doi:10.1021/acs.jpcc.6b06217

Velicky, M., Donnelly, G. E., Hendren, W. R., McFarland, S., Scullion, D., DeBenedetti, W. J., et al. (2018). Mechanism of gold-assisted exfoliation of centimeter-sized transition-metal dichalcogenide monolayers. *ACS Nano* 12, 10463–10472. doi:10.1021/acsnano.8b06101

Wu, K., Wang, H., Yang, M., Liu, L., Sun, Z., Hu, G., et al. (2024a). Gold-template-assisted mechanical exfoliation of large-area 2D layers enables efficient and precise construction of moiré superlattices. *Adv. Mater.* 36, 2313511. doi:10.1002/adma.202313511

Wu, K., Yang, Z., Shi, Y., Wang, Y., Xiang, B., Zhou, H., et al. (2024b). Revealing the optical transition properties of interlayer excitons in defective WS_2/WSe_2 heterobilayers. *Nano Lett.* 24, 8671–8678. doi:10.1021/acs.nanolett.4c02025

Wu, Q., Bagheri Tagani, M., Zhang, L., Wang, J., Xia, Y., Zhang, L., et al. (2022). Electronic tuning in WSe_2/Au via van der Waals interface twisting and intercalation. *ACS Nano* 16, 6541–6551. doi:10.1021/acsnano.2c00916

Xia, Y., Ding, D., Xiao, K., Zhang, J., Xu, S., He, D., et al. (2023). Wafer-scale single-crystalline $MoSe_2$ and WSe_2 monolayers grown by molecular-beam epitaxy at low-temperature—the role of island-substrate interaction and surface steps. *Nat. Sci.* 3, 20220059. doi:10.1002/ntls.20220059

Xing, X., Zhao, L., Zhang, W., Wang, Z., Su, H., Chen, H., et al. (2020). Influence of a substrate on ultrafast interfacial charge transfer and dynamical interlayer excitons in monolayer WSe_2/graphene heterostructures. *Nanoscale* 12, 2498–2506. doi:10.1039/c9nr09309e

Zatko, V., Galbiati, M., Dubois, S. M.-M., Och, M., Palczynski, P., Mattevi, C., et al. (2019). Band-structure spin-filtering in vertical spin valves based on chemical vapor deposited WS_2. *ACS Nano* 13, 14468–14476. doi:10.1021/acsnano.9b08178